

Article

Testing Cosmic Acceleration from the Late-Time Universe

Jose Agustin Lozano Torres 

Instituto de Física, Universidad Nacional Autónoma de México, Ciudad de México 04510, Mexico; jalozanotorres@gmail.com

Abstract: We investigate the accelerated cosmic expansion in the late universe and derive constraints on the values of the cosmic key parameters according to different cosmologies such as Λ CDM, w CDM, and w_0w_a CDM. We select 24 baryon acoustic oscillation (BAO) uncorrelated measurements from the latest galaxy surveys measurements in the range of redshift $z \in [0.106, 2.33]$ combined with the Pantheon SNIa dataset, the latest 33 $H(z)$ measurements using the cosmic chronometers (CCs) method, and the recent Hubble constant value measurement measured by Riess 2022 (R22) as an additional prior. In the Λ CDM framework, the model fit yields $\Omega_m = 0.268 \pm 0.037$ and $\Omega_\Lambda = 0.726 \pm 0.023$. Combining BAO with Pantheon plus the cosmic chronometers datasets we obtain $H_0 = 69.76 \pm 1.71 \text{ km s}^{-1} \text{ Mpc}^{-1}$ and the sound horizon result is $r_d = 145.88 \pm 3.32 \text{ Mpc}$. For the flat w CDM model, we obtain $w = -1.001 \pm 0.040$. For the dynamical evolution of the dark energy equation of state, w_0w_a CDM cosmology, we obtain $w_a = -0.848 \pm 0.180$. We apply the Akaike information criterion approach to compare the three models, and see that all cannot be ruled out from the latest observational measurements.

Keywords: dark energy; cosmological parameters; numerical methods

1. Introduction

The values and constraints of the cosmological parameters in the framework of Λ CDM cosmology have been estimated and highly constrained through various observational experiments [1,2] with unprecedented accuracy. The measurement results from Planck 2018 provide robust and detailed constraints for various cosmic parameters. In the Λ CDM scene, [1] measured the Hubble constant indirectly to be $H_0 = 67.4 \pm 0.5 \text{ km s}^{-1} \text{ Mpc}^{-1}$, with an uncertainty below $1 \text{ km s}^{-1} \text{ Mpc}^{-1}$. However, measurements of the Hubble constant in our local neighborhood at low redshifts ($z < 3$) performed by Riess et al. [3–7] have caused tension and, ironically, a window of opportunity to test alternative models beyond the Λ CDM model. In particular, the SH0ES project [4] developed a distance ladder method from standard candles known as Cepheid stars to estimate H_0 . They have been improving the precision of the value of H_0 and obtained the updated results as $H_0 = 73.04 \pm 1.04 \text{ km s}^{-1} \text{ Mpc}^{-1}$ in 2022 [7]. Although the Λ CDM model is widely accepted by the scientific community, the current measurements of late-time accelerated cosmic expansion [7] and early-time accelerated cosmic expansion [1] disagree with each other, causing a crisis in cosmology known as Hubble tension; the discrepancy between them is situated in the range of 4σ – 5.7σ . Such a discrepancy implies that either early- and late-time measurements have systematic and calibration issues or the standard cosmological model fails to describe the universe. Furthermore, this tension may provide a hint of new physics beyond the standard model. Following this motivation, a wide range of alternative models have been developed to alleviate inconsistencies between data surveys [8–20].

In the opposite case, many studies have been made to provide estimates of the Hubble constant based on other observations, such as quasar lensing [21,22], gravitational-wave events [23–25], fast radio bursts (FRBs) [26,27], megamasers [28–30], the red giant branch tip method (TRGS) [31–33], BAOs [34], etc. [35]. For example, the H0LiCOW research group [36] demonstrated another method to estimate H_0 via gravitational lensing effects. Under the Λ CDM



Citation: Lozano Torres, J.A. Testing Cosmic Acceleration from the Late-Time Universe. *Astronomy* **2023**, *2*, 300–314. <https://doi.org/10.3390/astronomy2040020>

Academic Editor: Ignatios Antoniadis

Received: 18 August 2023

Revised: 1 December 2023

Accepted: 11 December 2023

Published: 14 December 2023



Copyright: © 2023 by the author. Licensee MDPI, Basel, Switzerland. This article is an open access article distributed under the terms and conditions of the Creative Commons Attribution (CC BY) license (<https://creativecommons.org/licenses/by/4.0/>).

scenario, they obtained a value of $H_0 = 73.3^{+1.7}_{-1.8}$ km s⁻¹ Mpc⁻¹ [36]. The Advanced LIGO and Virgo research teams detected a gravitational-wave event GW170817 coming from a neutron-star merging system. They measured $H_0 = 70^{+12.0}_{-8.0}$ km s⁻¹ Mpc⁻¹ [24]. These observations present an advantage: they are independent from cosmic microwave background and distance ladder measurements, offering an answer to the observed H_0 tension. As for baryon acoustic oscillations (BAOs), which are a matter of interest in our study, they are sound waves traveling in the primordial plasma, frozen at the recombination epoch. These oscillations have been found in the spider's-web-like galactic structures by different independent observational surveys. The BAOs surveys give measurement results in terms of $D_A(z)/r_d$, $D_V(z)/r_d$, $D_M(z)/r_d$, D_H/r_d , $D_A(r_d/r_{d, fid})$, $D_V(r_d/r_{d, fid})$, and $H(z) \cdot r_d$, where r_d is the sound horizon distance at the drag epoch. In the recombination era, the photons depart from the baryon matter, at $z_* \approx 1090$, giving rise to the CMB. The baryons do not sense the dragging effect of photons until $z_d \approx 1059$, which sets the standard ruler for the BAOs. The Hubble constant H_0 and the sound horizon r_d are strongly related, forming the so-called $H_0 - r_d$ plane, linking the early- and late-time universe. In general, r_d is subject to the conditions of the early universe, hence constrained via early observations performed by Planck 2018 [37]. Instead of the calibration of r_d via early observations as per Planck, an alternative method is to combine BAO measurements with other low-redshift observations.

In this study, we select the final BAO measurement results from different observational experiments covering 24 BAO data points and test whether these BAO points could be correlated or not. According to [38], despite the existence of large galaxy survey datasets, it is recommended to use a small sample to minimize correlations among the selected data points, thus reducing the errors. One way is to examine the concordance of this subsample is incorporating random correlations and perform the analysis on the cosmological parameters. Furthermore, in our study we take into account the Λ CDM, w CDM, and w_0w_a CDM cosmological models. Combining the latest BAO measurements with the Pantheon SNeIA dataset, the cosmic chronometers dataset, and the latest measurement of the Hubble constant obtained by Riess 2022 as an additional prior [7], we estimate the r_d and H_0 parameters. The structure of the paper is the following: In Section 2, we present the cosmological models under study. The datasets and methodology are explained in Section 3. In Section 4, we present our estimated results from the latest low-redshift survey datasets. In Section 5, we present our results and their implications for the cosmological models under study.

2. Theoretical Background

2.1. Standard Cosmological Model

The Λ cold dark matter (Λ CDM) model takes the dark energy equation of state (EoS) as the cosmological constant Λ with $w = -1$, acting as a negative pressure to counteract the effect of gravity. The Friedmann equation for this model is expressed as

$$E^2(z) = \Omega_{r0}(1+z)^4 + \Omega_{m0}(1+z)^3 + \Omega_{DE}(z), \quad (1)$$

where we can set $\Omega_{DE}(z) = \Omega_\Lambda$, with EOS $w = -1$. The Friedmann equation (1) depends on the free parameters Ω_r , Ω_m , Ω_Λ . Although the radiation parameter Ω_r is usually not considered for a flat late-universe, we include it for a complete description. The term $E(z)$ is the function rate and is the ratio $H(z)/H_0$, where $H(z) = \dot{a}/a$ is the Hubble parameter at redshift z and H_0 is the Hubble constant measured at present time.

2.2. Flat Constant w CDM Model

The cosmological model w CDM assumes a constant EoS w . The Friedmann equation for w CDM model is expressed as

$$E^2(z) = \Omega_{r0}(1+z)^4 + \Omega_{m0}(1+z)^3 + \Omega_\Lambda(1+z)^{3(1+w(z))}, \quad (2)$$

where Equation (2) depends on the free parameters Ω_r , Ω_m , Ω_Λ , and $w(z)$.

2.3. CPL Parametrization

The dark energy EoS w can be treated as a function of the cosmic time translated in redshift z or scale factor $a(t)$ of the FLRW metric universe, noting that $1 + z = a_0/a(t)$, where $a_0 = 1$ given by the current time. Here, we consider a dynamical EoS w parametrization called the Chevallier–Polarski–Linder (CPL) model. This model introduces a parametrization that varies as a function of time. This model is given by [39–41]

$$w(a) = w_0 + (1 - a)w_a, \quad (3)$$

or in terms of redshift z ,

$$w(z) = w_0 + w_a \frac{z}{1+z}, \quad (4)$$

where w_0 represents the cosmological constant Λ or the current value of EoS, that means, $w(z = 0) = w_0$, and noting that $(\frac{dw(z)}{dz})_{z=0} = w_a$, one can regard this as a free time parameter. From the CPL parametrization, we can write the Friedmann equation in terms of the expansion function as

$$E^2(z) = \Omega_r(1+z)^4 + \Omega_m(1+z)^3 + \Omega_{DE}(1+z)^{3(1+w_0+w_a)} \exp\left(-\frac{3w_a z}{1+z}\right), \quad (5)$$

where Equation (5) depends on the free parameters Ω_r , Ω_m , Ω_Λ , w_0 , and w_a . The measured values of redshift and angles on the celestial sphere need to be translated into cosmological distances by setting a fiducial model, estimating the ratio of the observed BAO scale to that predicted in the fiducial model. The studies of the BAO feature in the transverse direction provide a measurement of $D_H(z)/r_d = c/H(z)r_d$, with the comoving angular diameter distance in a flat space,

$$D_M = \frac{c}{H_0} \int_0^z \frac{dz'}{E(z')}. \quad (6)$$

Furthermore, the BAO data are also expressed in cosmological observables such as $D_A = D_M/(1+z)$ and $D_V(z)/r_d$, which encodes the BAO peak coordinates information,

$$D_V(z) = [zD_H(z)D_M^2(z)]^{1/3}, \quad (7)$$

where r_d is the sound horizon distance at the drag epoch measured by [1] in $r_d = 147.1$ Mpc.

3. Data and Methodology

For our analysis we select a subset of data points of the latest BAO measurements from different galaxy survey experiments. The data points mainly come from the Sloan Digital Sky Survey (SDSS) [42–47]. In addition, we also include data measurements from the Dark Energy Survey (DES) [48], the Dark Energy Camera Legacy Survey (DECaLS) [49], and 6dFGS BAO [50]. The BAO data points are listed in Table 1 with their corresponding redshifts z_{eff} , observables, measurements, and errors. Although we choose a subset of data points from a huge set of BAO data points to avoid highly correlated data points, it is still possible that our subset of data points listed in Table 1 can exhibit correlations between the different measurements in the data releases. To estimate the systematic error, one needs to use mocks based on N-body simulations to find out the correct covariance matrices. Since we use a collection of measurements from different observational surveys, we do not use a precise covariance matrix between them. To overcome this issue, we follow the covariance analysis given in [38]. The covariance matrix for uncorrelated points is

$$C_{ii} = \sigma_i^2. \quad (8)$$

To simulate the impact of correlations in our subsample listed in Table 1, we can incorporate a certain number of non-diagonal elements randomly in the covariance matrix while keeping it symmetric. Based on this method, we establish non-negative correlations

in up to twelve pairs of aleatory data points, which represents 50% of the BAO dataset given in Table 1. The locations of the non-diagonal elements are selected as aleatory and their magnitudes are set to

$$C_{ij} = 0.5\sigma_i\sigma_j, \quad (9)$$

where $\sigma_i\sigma_j$ are the 1σ errors of the data points i, j . We implemented a nested sampling algorithm tailored for high-dimensional parameter space called *Polychord*, developed by [51], to perform the calculations. The prior we selected was with a uniform distribution given by

$$\Omega_m \in [0.;1], \quad \Omega_{DE} \in [0.;1 - \Omega_m], \quad H_0 \in [50;100], \quad r_d \in [100;200]\text{Mpc} \quad (10)$$

In the case of the fiducial cosmology, we selected as a prior for the ratio $r_d/r_{fid} \in [0.9, 1.1]$. Furthermore, the latest measurement of the Hubble constant estimated by Riess in 2022 [7] and confirmed with the observations carried out by the James Webb space telescope (JWST) [52] $H_0 = 73.04 \pm 1.04 \text{ km s}^{-1} \text{ Mpc}^{-1}$ was integrated into our analysis as an additional Gaussian prior, we refer to it as R22. The “full-dataset” encodes the sum of the BAO + CC + Pantheon datasets.

Table 1. Sample of 24 BAO uncorrelated data points on which we perform our analysis. Our data points mainly come from the final measurements of the SDSS-III BOSS-DR12 and SDSS-IV eBOSS-DR16 samples for strengthening our results.

z_{eff}	Observable	Measurement	Error	Year	Dataset Survey	Reference
0.106	r_d/D_V	0.336	0.015	2011	6dFGS BAO	[50]
0.15	D_V/r_d	4.47	0.17	2021	SDSS Main Galaxy Sample	[53]
0.31	D_A/r_d	6.29	0.14	2017	SDSS-III BOSS-DR12	[54]
0.36	D_A/r_d	7.09	0.16	2017	SDSS-III BOSS-DR12	[54]
0.38	D_H/r_d	25.00	0.76	2021	SDSS BOSS Galaxy Sample	[54]
0.40	D_A/r_d	7.70	0.16	2017	SDSS-III BOSS-DR12	[54]
0.44	D_A/r_d	8.20	0.13	2017	SDSS-III BOSS-DR12	[54]
0.48	D_A/r_d	8.64	0.11	2017	SDSS-III BOSS-DR12	[54]
0.51	D_M/r_d	13.36	0.21	2021	SDSS BOSS Galaxy Sample	[53]
0.52	D_A/r_d	8.90	0.12	2017	SDSS-III BOSS-DR12	[54]
0.56	D_A/r_d	9.16	0.14	2017	SDSS-III BOSS-DR12	[54]
0.59	D_A/r_d	9.45	0.17	2017	SDSS-III BOSS-DR12	[54]
0.64	D_A/r_d	9.62	0.22	2017	SDSS-III BOSS-DR12	[54]
0.697	$D_A(r_d/r_{d,fid})$	1529	73	2020	DECaLS DR8 Footprint LRG	[49]
0.698	D_H/r_d	19.77	0.47	2020	eBOSS DR16 LRG Sample	[44]
0.698	D_M/r_d	17.65	0.30	2020	eBOSS DR16 LRG Sample	[44]
0.70	D_M/r_d	17.96	0.51	2021	eBOSS DR16 ELG Sample	[55]

Table 1. Cont.

z_{eff}	Observable	Measurement	Error	Year	Dataset Survey	Reference
0.835	D_M/r_d	18.92	0.51	2022	Dark Energy Survey Year 3	[48]
0.845	D_H/r_d	20.91	2.86	2021	eBOSS DR16 ELG Sample	[55]
0.874	$D_A(r_d/r_{d, fid})$	1680	109	2020	DECaLS DR8 Footprint LRG	[49]
1.48	D_H/r_d	13.23	0.47	2021	eBOSS DR16 Quasar Sample	[46]
1.48	D_M/r_d	30.21	0.79	2021	eBOSS DR16 Quasar Sample	[46]
2.33	D_H/r_d	8.99	0.19	2020	eBOSS DR16 Ly α -Quasar	[47]
2.33	D_M/r_d	37.5	1.1	2020	eBOSS DR16 Ly α -Quasar	[47]

4. Analysis and Results

In order to constraint our models, aside from the collection of BAO data points listed in Table 1, we use the Pantheon dataset given in [56], the latest Hubble parameter $H(z)$ measurements using the cosmic chronometers (CCs) method containing 33 uncorrelated data points listed in Table 2, and the latest Hubble constant measurement, labeled as R22 [7], as an additional Gaussian prior.

Table 2. The latest 33 $H(z)$ measurements (in units of $\text{km s}^{-1} \text{Mpc}^{-1}$) obtained with the CC method and their associated errors on which we perform our analysis. It is noted that all these measurements are independent, since they come from different datasets.

z	$H(z)$	$\sigma_{H(z)}$	Method	Reference
0.07	69	19.6	Full-spectrum fitting	[57]
0.09	69	12	Full-spectrum fitting	[58]
0.12	68.6	26.2	Full-spectrum fitting	[57]
0.17	83	8	Full-spectrum fitting	[58]
0.179	75	4	Calibrated D4000	[59]
0.199	75	5	Calibrated D4000	[59]
0.20	72.9	29.6	Full-spectrum fitting	[57]
0.27	77	14	Full-spectrum fitting	[58]
0.28	88.8	36.6	Full-spectrum fitting	[57]
0.352	83	14	Calibrated D4000	[59]
0.38	83	13.5	Calibrated D4000	[60]
0.4	95	17	Full-spectrum fitting	[58]
0.4004	77	10.2	Calibrated D4000	[60]
0.425	87.1	11.2	Calibrated D4000	[60]
0.445	92.8	12.9	Calibrated D4000	[60]
0.47	89.0	49.6	Full-spectrum fitting	[61]
0.4783	80.9	9	Calibrated D4000	[60]
0.48	97	62	Full-spectrum fitting	[62]
0.593	104	13	Calibrated D4000	[59]
0.68	92	8	Calibrated D4000	[59]
0.75	98.8	33.6	Lick indices	[63]
0.781	105	12	Calibrated D4000	[59]
0.80	113.1	28.5	Full-spectrum fitting	[64]
0.875	125	17	Calibrated D4000	[59]
0.88	90	40	Full-spectrum fitting	[62]
0.9	117	23	Full-spectrum fitting	[58]
1.037	154	20	Calibrated D4000	[59]
1.3	168	17	Full-spectrum fitting	[58]
1.363	160	33.6	Calibrated D4000	[65]
1.43	177	18	Full-spectrum fitting	[58]
1.53	140	14	Full-spectrum fitting	[58]
1.75	202	40	Full-spectrum fitting	[58]
1.965	186.5	50.4	Calibrated D4000	[65]

The results for the BAO and the BAO+R22 in the context of test random correlations are depicted in Figure 1 and listed in Table 3. Introducing some random correlations changes the values of the cosmological parameters Ω_m and Ω_Λ . However, the difference between no correlation ($n = 0$) and 50% correlated points ($n = 12$) is surprisingly about 5%, allowing us to consider our BAO dataset uncorrelated, which is very low compared to the discrepancy given in [38].

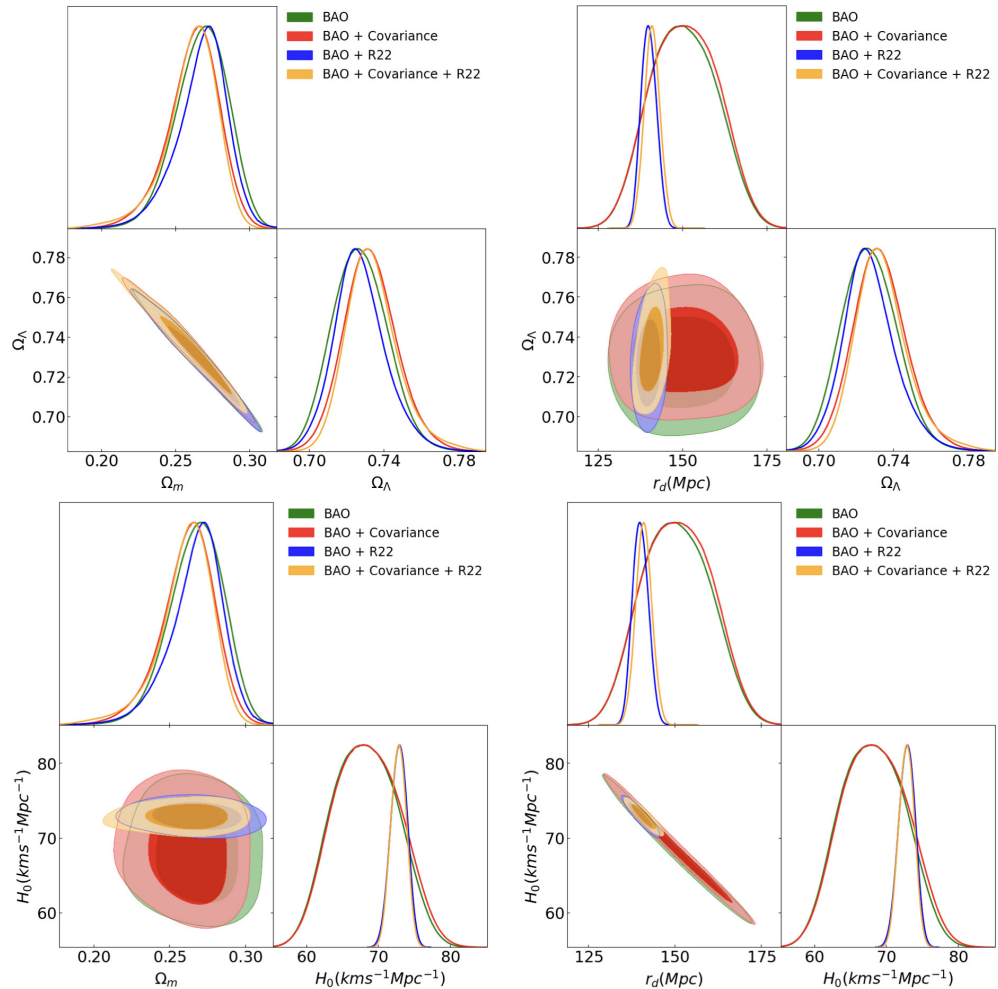


Figure 1. The constraints of the posterior distributions for Λ CDM with and without a test random covariance matrix with twelve components. The distribution with covariance matrix between null and twelve components is almost negligible, nearly indistinguishable from the uncorrelated dataset.

Table 3. Variation of some cosmological parameters according to the number of correlated pairs. The values with uncorrelated pairs ($n = 0$) are slightly different when $n = 6$ and $n = 12$ random correlated pairs are introduced.

n Correlated Pairs	BAO	BAO + R22
$n = 0$	$\Omega_m = 0.269 \pm 0.015$ $\Omega_\Lambda = 0.725 \pm 0.011$	$\Omega_m = 0.269 \pm 0.017$ $\Omega_\Lambda = 0.725 \pm 0.013$
$n = 6$	$\Omega_m = 0.263 \pm 0.015$ $\Omega_\Lambda = 0.731 \pm 0.015$	$\Omega_m = 0.264 \pm 0.015$ $\Omega_\Lambda = 0.730 \pm 0.014$
$n = 12$	$\Omega_m = 0.262 \pm 0.017$ $\Omega_\Lambda = 0.732 \pm 0.012$	$\Omega_m = 0.263 \pm 0.015$ $\Omega_\Lambda = 0.732 \pm 0.011$

4.1. Standard Cosmological Model

We can start evaluating the cosmological models based on the data measurements. For the Λ CDM model we vary the following parameters: H_0 , Ω_m , Ω_Λ , r_d , and r_d/r_{fid} . The estimated values of our varied parameters in the Λ CDM scenario for different combinations of datasets can be depicted in Figure 2, including the contours of the $\Omega_m - H_0$ and $H_0 - r_d$ planes.

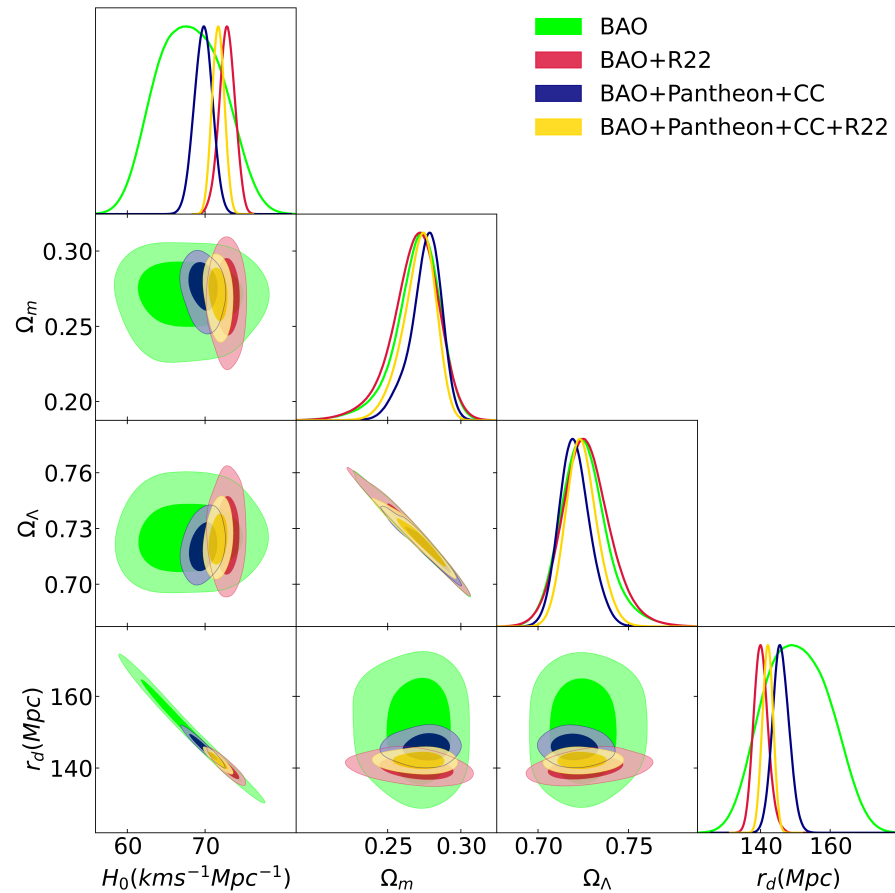


Figure 2. The constraints on the parameters using different observational data measurements in the Λ CDM model with 1σ and 2σ . BAO refers to the baryon acoustic oscillations dataset from Table 1. CC refers to the Hubble measurements based on the cosmic chronometers method listed in Table 2 and Pantheon refers to the SNeIa dataset. R22 denotes the measurement of the Hubble constant as a Gaussian prior [7].

In Figure 2, the 68% and 95% confidence levels for the posterior distribution of some of the cosmological key parameters of the standard Λ CDM model are reported. The numerical results of the evaluated cosmological parameters are listed in Table 4. When the BAO dataset alone is regarded, our estimated values of H_0 and r_d are closely in agreement with those obtained by Planck 2018 [1]. However, our estimated values of matter density Ω_m and dark energy density Ω_Λ are smaller than the values reported in [1]. When we combine the R22 prior for H_0 , the fit gives an estimated value for H_0 away from [1] and closer to the one measured in the SNe sample by [7]. On the other hand, when we have the full dataset (BAO + Pantheon + CC), the value of the Hubble constant is closer to that value estimated by [1]. We also observe that the matter–energy densities are smaller to the values estimated by [1] ($\Omega_m = 0.315 \pm 0.007$, $\Omega_\Lambda = 0.685 \pm 0.007$), but this observation has been reported in other studies [66,67]. In the framework of the BAO scale, it is set by the cosmic sound

horizon imprinted in the cosmic microwave background at the drag epoch z_d when the sea of baryons and photons decouple from each other, according to

$$r_d = \int_{z_d}^{\infty} \frac{c_s(z)}{H(z)} dz, \quad (11)$$

where the speed of sound is expressed as $c_s = \sqrt{\frac{\delta p_\gamma}{\delta \rho_B + \delta \rho_\gamma}} = \sqrt{\frac{(1/3)\delta p_\gamma}{\delta \rho_B + \delta \rho_\gamma}} = \frac{1}{\sqrt{3(1+R)}}$, where $R \equiv \delta \rho_B / \delta \rho_\gamma = \frac{3\rho_B}{4\rho_\gamma}$. The data from [1] gives the redshift at the drag epoch $z_d = 1059.94 \pm 0.30$. For a flat Λ CDM, the measurements in [1] estimate $r_d = 147.09 \pm 0.26$ Mpc. In our analysis, the posterior distribution of the $r_d - H_0$ contour plane is shown at the bottom of the first column in Figure 2. We find for the full dataset $r_d = 145.88 \pm 3.32$ Mpc, close to the Planck results. Adding the Riess 2022 prior into the full dataset gives $r_d = 142.10 \pm 2.49$ Mpc. Ref. [68] finds $r_d = 143.9 \pm 3.1$ Mpc. Ref. [69] reports that using binning and Gaussian methods to combine measurements of the 2D BAO and SNe data, the values of the absolute BAO scale range from $141.45 \text{ Mpc} \leq r_d \leq 159.44 \text{ Mpc}$ (binning) and $143.35 \text{ Mpc} \leq r_d \leq 161.59 \text{ Mpc}$ (Gaussian). The above results demonstrate a clear discrepancy between early- and late-time observational measurements, analogously to the H_0 tension. It should be noticed that our results depend on the range of priors for r_d and H_0 , shifting the estimated values in the $r_d - H_0$ contour plane. A noticeable feature is that when we do not include the Riess 2022 prior the results of H_0 and r_d tend to be in agreement with the Planck and SDSS results.

Table 4. Constraints at 95% CL on the cosmological parameters for the standard Λ CDM model based on the baryon acoustic oscillations dataset (BAO) listed in Table 1, the Hubble measurements based on cosmic chronometers (CCs) method listed in Table 2, Pantheon dataset, and additional Gaussian prior R22.

Parameter	BAO	BAO + R22	BAO + Pantheon + CC	BAO + Pantheon + CC + R22
H_0 (km s ⁻¹ Mpc ⁻¹)	68.01 ± 4.53	72.82 ± 1.01	69.76 ± 1.71	71.68 ± 1.65
Ω_m	0.270 ± 0.039	0.268 ± 0.037	0.275 ± 0.025	0.271 ± 0.026
Ω_Λ	0.725 ± 0.022	0.726 ± 0.023	0.720 ± 0.014	0.724 ± 0.015
r_d (Mpc)	150.45 ± 9.89	140.14 ± 3.16	145.88 ± 3.32	142.10 ± 2.49
r_d/r_{fid}	0.999 ± 0.074	0.938 ± 0.023	0.971 ± 0.028	0.949 ± 0.024

4.2. Models beyond Standard Model

Aside from the standard Λ CDM cosmological model, we test two more cosmological models whose dark energy EoSs are non-dynamical, dynamical, and different from $w = -1$: the w CDM model and the $w_0 w_a$ CDM model. For the w CDM model, we use $w \in [-1.25; -0.5]$, while for the $w_0 w_a$ CDM model, we use $w_0 \in [-1.25; -0.5]$ and $w_a \in [1.0; -1.0]$. The rest of the priors are the same as for the Λ CDM model.

4.2.1. w CDM Model

This model considers a fixed dark energy equation of state $w \neq -1$. The results for different combinations of dataset surveys are depicted in Figure 3 and listed in Table 5. From our results, the dark energy EoS is similar to the cosmological constant Λ for the full dataset: $w = -1.001 \pm 0.040$; and in agreement with [1] ($w = -1.03 \pm 0.03$) when taking into account the full dataset BAO+CC+Pantheon plus Riess 2022 (R22): $w = -1.014 \pm 0.053$. On the other hand, when we consider the BAO and BAO+R22 datasets, the EoS is $w > -1$.

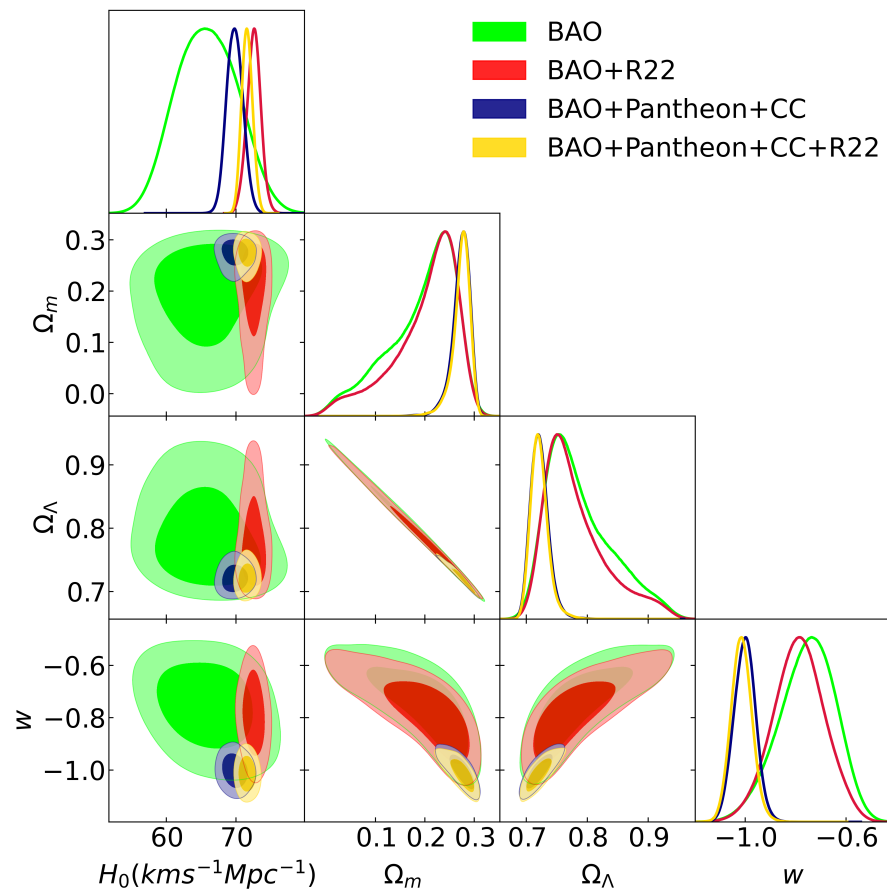


Figure 3. The posterior distributions for different observational data measurements with the w CDM model with 1σ and 2σ . BAO refers to the baryon acoustic oscillations dataset from Table 1. CC refers to the cosmic chronometers and Pantheon refers to the Hubble diagram from SNeIa. R22 denotes the Riess 2022 measurement of the Hubble constant as a Gaussian prior [7].

Table 5. Constraints at 95% CL on the cosmological parameters for the w CDM model based on baryon acoustic oscillations (BAOs), cosmic chronometers (CCs), Pantheon, and additional Gaussian prior R22.

Parameter	BAO	BAO + R22	BAO + Pantheon + CC	BAO + Pantheon + CC + R22
H_0 (km s ⁻¹ Mpc ⁻¹)	65.83 ± 4.73	72.56 ± 2.10	69.83 ± 1.06	71.60 ± 1.02
Ω_m	0.193 ± 0.077	0.201 ± 0.068	0.273 ± 0.015	0.273 ± 0.016
Ω_Λ	0.786 ± 0.050	0.780 ± 0.046	0.721 ± 0.013	0.721 ± 0.013
w	-0.753 ± 0.168	-0.786 ± 0.210	-1.001 ± 0.040	-1.014 ± 0.053
r_d (Mpc)	150.67 ± 10.32	136.90 ± 2.48	145.73 ± 3.45	142.44 ± 2.24
r_d/r_{fid}	0.996 ± 0.069	0.924 ± 0.018	0.970 ± 0.029	0.949 ± 0.025

The above results imply that we cannot rule out $w = -1$ when we consider the full dataset and full dataset plus R22. In Figure 4, we observe the $r_d - H_0$ plane in the framework of the w CDM model.

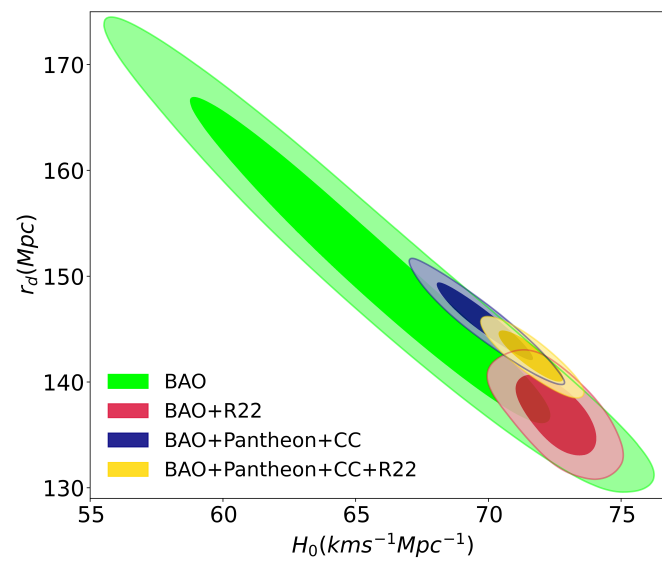


Figure 4. The posterior distributions for different observational data measurements of w CDM model with 1σ and 2σ in the $r_d - H_0$ contour plane. The BAO refers to the baryon acoustic oscillations dataset from Table 1. The CC dataset refers to the cosmic chronometers and Pantheon refers to the Hubble diagram from SNeIa. R22 denotes [7] measurement of the Hubble constant as a Gaussian prior.

We observe that the sound horizon distance value from the full-dataset and BAO dataset alone are in agreement with the value estimated by [1]. However, when we incorporate R22 into the full-dataset and BAO dataset alone the sound horizon at drag epoch yields $r_d = 142.73 \pm 2.74$ Mpc and $r_d = 138.26 \pm 2.82$ Mpc, respectively. Although these values are in tension with the r_d value estimated by Planck, our estimated results with Riess 2022 are clearly in agreement with those obtained by [68] $r_d = 143.9 \pm 3.1$ Mpc, [66] independent of CMB data $r_d = 144 \pm_{-5.5}^{+5.3}$ Mpc (from $\theta_{BAO} + BBN + HoLiCOW$), and [70] $r_d = 143.7 \pm 2.7$ Mpc.

4.2.2. w_0w_a CDM Model

Our estimated value of the w_a parameter for different datasets combinations are depicted in Figure 5 and listed in Table 6. It is interesting to observe that our value is nearly in agreement with the one obtained by [1] with TT, TE, EE + lowE + lensing with other datasets: $w_a = -0.72^{+0.62}_{-0.54}$ (from *Planck* + BAO/RSD + WL) even though we take different combinations of datasets. The $r_d - H_0$ plane in the framework of w_0w_a CDM model is presented in Figure 6.

Table 6. Constraints at 95% CL on the cosmological parameters for the w_0w_a CDM model based on baryon acoustic oscillations (BAOs), cosmic chronometers (CCs), Pantheon-QSR-GRB, and additional prior R22.

Parameters	BAO	BAO + R22	BAO + Pantheon + CC	BAO + Pantheon + CC + R22
H_0 (km s ⁻¹ Mpc ⁻¹)	65.82 ± 4.43	72.83 ± 1.41	69.90 ± 1.06	71.71 ± 1.06
Ω_m	0.159 ± 0.098	0.165 ± 0.073	0.183 ± 0.056	0.178 ± 0.050
Ω_Λ	0.826 ± 0.080	0.820 ± 0.065	0.810 ± 0.050	0.814 ± 0.050
w_0	-1.214 ± 0.130	-1.149 ± 0.121	-1.027 ± 0.069	-1.020 ± 0.072
w_a	-0.344 ± 0.432	-0.478 ± 0.390	-0.848 ± 0.180	-0.878 ± 0.161
r_d (Mpc)	152.01 ± 10.18	138.26 ± 2.82	146.18 ± 2.35	142.73 ± 2.36
r_d/r_{fid}	1.002 ± 0.066	0.930 ± 0.022	0.974 ± 0.033	0.950 ± 0.035

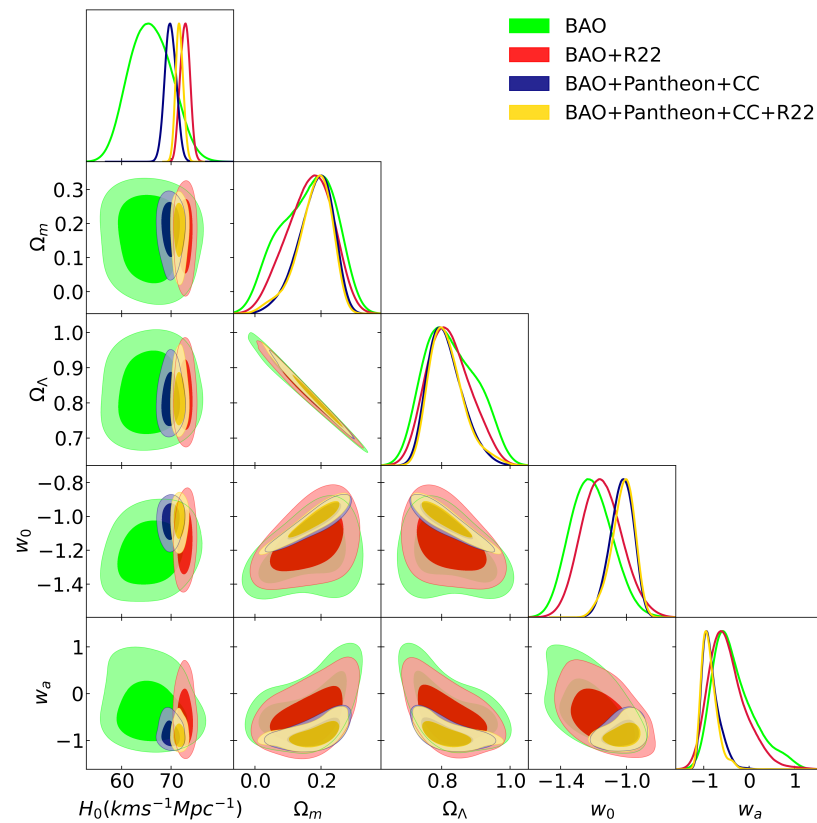


Figure 5. The posterior distributions for different observational data measurements with the w_0w_a CDM model with 1σ and 2σ . BAO represents the dataset given in Table 1. CC represents the dataset given in Table 2, and Pantheon refers to the Hubble diagram from SNeIa. R22 denotes [7] measurement of the Hubble constant as a Gaussian prior.

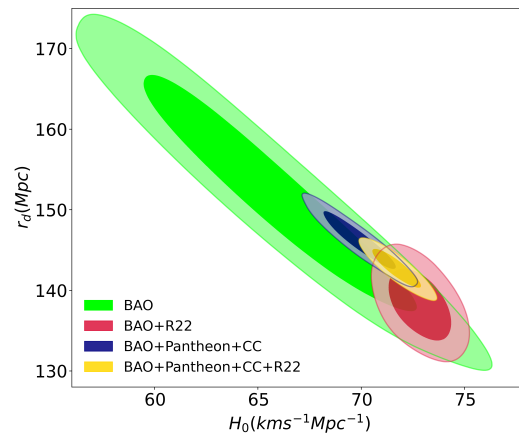


Figure 6. The figure exhibits the posterior distributions for different observational data measurements with the w_0w_a CDM with 1σ and 2σ in the $r_d - H_0$ contour plane. BAO refers to the baryon acoustic oscillations dataset in Table 1. CC refers to the cosmic chronometers dataset listed in Table 2, and Pantheon refers to the Hubble diagram from SNeIa. R22 denotes Riess 2022 measurement of the Hubble constant [7].

The fit for the BAO dataset alone leads to $r_d = 152.01 \pm 10.18$ Mpc. Adding the CC and Pantheon datasets r_d results in 146.18 ± 2.35 Mpc, staying in agreement with [1]. And including the R22 prior into the full dataset leads to $r_d = 142.73 \pm 2.36$, smaller to that estimated by Planck, but in agreement with other studies [66,67,70].

5. Discussion

Our study selected 24 data points that represent the latest and final BAO measurements from different observational surveys in the last two decades in combination with the dataset of $H(z)$ measurements using the cosmic chronometers method (33 data points), the Pantheon SNeIa dataset (40 data points), and the latest measurement of the Hubble constant made by Riess 2022. Although our results based on the latest measurements from different observational tests demonstrate that the Hubble tension is still there it has been alleviated: 2σ for the H_0 . By introducing the sound horizon r_d as a free parameter we find for the full dataset (BAO + Pantheon + CC) $H_0 = 69.76 \pm 1.71 \text{ km s}^{-1} \text{ Mpc}^{-1}$ and $r_d = 145.88 \pm 3.32 \text{ Mpc}$ in the Λ CDM model, $H_0 = 69.83 \pm 1.06 \text{ km s}^{-1} \text{ Mpc}^{-1}$ and $r_d = 145.73 \pm 3.45 \text{ Mpc}$ in the w CDM model, and $H_0 = 69.90 \pm 1.06 \text{ km s}^{-1} \text{ Mpc}^{-1}$ and $r_d = 146.18 \pm 2.35 \text{ Mpc}$ in the w_0w_a CDM model. To compare our different cosmological models, we apply the Akaike information criterion (AIC) and the Bayesian information criterion (BIC). The Akaike information criterion is defined as [71]

$$\text{AIC} = -2\ln(\mathcal{L}_{max}) + 2k + \frac{2k(2k+1)}{N_{tot} - k - 1}, \quad (12)$$

where \mathcal{L}_{max} is the maximum likelihood of the data taken into consideration in which we take the full dataset without the Riess 2022 prior, N_{tot} is the total number of data points, and k is the numbers of parameters. For large N_{tot} , our expression is reduced to

$$\text{AIC} \simeq -2\ln(\mathcal{L}_{max}) + 2k, \quad (13)$$

which is the standard form of the AIC criterion [71]. On the other hand, the Bayesian information criterion is defined as [72]

$$\text{BIC} = -2\ln(\mathcal{L}_{max}) + k\ln N_{tot}. \quad (14)$$

Thus, we can calculate the AIC and BIC for the standard Λ CDM, w CDM, and w_0w_a CDM models. We find for Λ CDM, w CDM, and w_0w_a CDM, $\text{AIC} = 98.0, 100.7,$ and $98.6,$ respectively. On the other hand, we find $\text{BIC} = 97.9, 100.6,$ and $98.5,$ respectively. Although the Λ CDM model has the best fit due the lowest AIC, our AIC and BIC values clearly show a good support in favor of all our tested models and cannot be ruled out from the current data.

Referring to our results, we see that the values of the Hubble constant H_0 and the sound horizon distance r_d based on low-redshift measurements (BAO + Pantheon + CC), are in agreement with the early measurements estimated by Planck [1], even though the dark energy and matter densities are lower. Therefore, in our analysis, the tension between low-redshift and high-redshift r_d measurements is not exhibited here in all our cosmological models as long as we do not include the Riess 2022 prior. Furthermore, it is striking that, based on the full dataset, we see that $w \approx -1$, taking the form of the cosmological constant Λ and in agreement with Planck [1] and closely to the result obtained by [53]. Our analysis and results show the robustness of the Λ CDM, w CDM, and w_0w_a CDM models based on our full dataset, showing consistency with the Planck measurements for H_0 and r_d . Although the R22 prior changes the values of H_0 and r_d , creating a tension, they still agree with other studies [66,67,69].

Funding: This research received no external funding.

Institutional Review Board Statement: Not applicable.

Informed Consent Statement: Not applicable.

Data Availability Statement: The data underlying this article is already given with references during the analysis of this work.

Acknowledgments: We would like to thank CONAHCYT for sponsoring this project.

Conflicts of Interest: The author declares no conflict of interest. The funders had no role in the design of the study; in the collection, analyses, or interpretation of data; in the writing of the manuscript; or in the decision to publish the results.

References

1. Planck Collaboration. Planck 2018 Results—VI. Cosmological Parameters. *Astron. Astrophys.* **2020**, *A6*, 641.
2. Bennett, C.L.; Larson, D.; Weil, J.L.; Jarosik, N.; Hinshaw, G.; Odegard, N.; Smith, K.M.; Hill, R.S.; Gold, B.; Halpern, M.; et al. Nine-year Wilkinson microwave anisotropy probe (WMAP) observations: Final maps and results. *Astrophys. J. Suppl. Ser.* **2013**, *208*, 20. [[CrossRef](#)]
3. Riess, A.G.; Filippenko, A.V.; Challis, P.; Clocchiatti, A.; Diercks, A.; Garnavich, P.M.; Gillil, R.L.; Hogan, C.J.; Jha, S.; Kirshner, R.P.; et al. Observational Evidence from Supernovae for an Accelerating Universe and a Cosmological Constant. *Astron. J.* **1998**, *116*, 1009. [[CrossRef](#)]
4. Riess, A.G.; Macri, L.; Casertano, S.; Lampeitl, H.; Ferguson, H.C.; Filippenko, A.V.; Jha, S.W.; Li, W.; Chornock, R. A 3% solution: Determination of the Hubble constant with the Hubble space telescope and wide field camera 3. *Astron. J.* **2011**, *730*, 119. [[CrossRef](#)]
5. Riess, A.G.; Macri, L.M.; Hoffmann, S.L.; Scolnic, D.; Casertano, S.; Filippenko, A.V.; Tucker, B.E.; Reid, M.J.; Jones, D.O.; Silverman, J.M.; et al. A 2.4% determination of the local value of the Hubble constant. *Astron. J.* **2016**, *826*, 56. [[CrossRef](#)]
6. Riess, A.G.; Casertano, S.; Yuan, W.; Macri, L.M.; Scolnic, D. Large Magellanic Cloud Cepheid Standards Provide a 1% Foundation for the Determination of the Hubble Constant and Stronger Evidence for Physics beyond Λ CDM. *Astron. J.* **2019**, *876*, 55. [[CrossRef](#)]
7. Riess, A.G.; Yuan, W.; Macri, L.M.; Scolnic, D.; Brout, D.; Casertano, S.; Jones, D.O.; Murakami, Y.; Anand, G. S.; Breuval, L.; et al. A Comprehensive Measurement of the Local Value of the Hubble Constant with 1 km/s/Mpc Uncertainty from the Hubble Space Telescope and the SH0ES Team. *Astrophys. J. Lett.* **2022**, *934*, L7. [[CrossRef](#)]
8. Huang, Q.G.; Wang, K. How the dark energy can reconcile Planck with local determination of the Hubble constant. *Eur. Phys. J.* **2016**, *76*, 506. [[CrossRef](#)]
9. Di Valentino, E.; Melchiorri, A.; Silk, J. Reconciling Planck with the local value of H_0 in extended parameter space. *Phys. Lett. B* **2016**, *761*, 242–246. [[CrossRef](#)]
10. Xu, L.; Huang, Q.G. Detecting the neutrinos mass hierarchy from cosmological data. *Sci. China Phys. Mech. Astron.* **2018**, *61*, 039521. [[CrossRef](#)]
11. Yang, W.; Pan, S.; Di Valentino, E.; Saridakis, E.N.; Chakraborty, S. Observational constraints on one-parameter dynamical dark-energy parametrizations and the H_0 tension. *Phys. Rev. D* **2019**, *99*, 043543. [[CrossRef](#)]
12. Poulin, V.; Smith, T.L.; Karwal, T.; Kamionkowski, M. Early Dark Energy can Resolve the Hubble Tension. *Phys. Rev. Lett.* **2019**, *122*, 221301. [[CrossRef](#)] [[PubMed](#)]
13. Vagnozzi, S. New physics in light of the H_0 tension: An alternative view. *Phys. Rev. D* **2020**, *102*, 023518. [[CrossRef](#)]
14. Liu, M.; Huang, Z.; Luo, X.; Miao, H.; Singh, N.K.; Huang, L. Can non-standard recombination resolve the Hubble tension? *Sci. China Phys. Mech. Astron.* **2020**, *63*, 290405. [[CrossRef](#)]
15. Ding, Q.; Nakama, T.; Wang, Y. A gigaparsec-scale local void and the Hubble tension. *Sci. China Phys. Mech. Astron.* **2020**, *63*, 290403. [[CrossRef](#)]
16. Ryan, J.; Chen, Y.; Ratra, B. Baryon acoustic oscillation, Hubble parameter, and angular size measurement constraints on the Hubble constant, dark energy dynamics, and spatial curvature. *Mon. Not. R. Astron. Soc.* **2019**, *488*, 3844–3856. [[CrossRef](#)]
17. Zhao, G.B.; Raveri, M.; Pogosian, L.; Wang, Y.; Crittenden, R.G.; Handley, W.J.; Percival, W.J.; Beutler, F.; Brinkmann, J.; Chuang, C.; et al. Dynamical dark energy in light of the latest observations. *Nat. Astron.* **2017**, *1*, 627–632. [[CrossRef](#)]
18. Li, X.; Shafieloo, A. A Simple Phenomenological Emergent Dark Energy Model can Resolve the Hubble Tension. *Astrophys. J. Lett.* **2019**, *883*, L3. [[CrossRef](#)]
19. Di Valentino, E. Investigating Cosmic Discordance. *Astrophys. J. Lett.* **2021**, *908*, L9. [[CrossRef](#)]
20. Haitao, M.; Zhiqi, H. The H_0 Tension in Non-flat QCDM Cosmology. *Astron. J.* **2018**, *868*, 20.
21. Millon, M.; Galan, A.; Courbin, F.; Treu, T.; Suyu, S. H.; Ding, X.; Birrer, S.; Chen, G. C.-F.; Shajib, A. J.; Sluse, D.; et al. An exploration of systematic uncertainties in the inference of H_0 from time-delay cosmography. *Astron. Astrophys.* **2020**, *639*, A101. [[CrossRef](#)]
22. Wong, K.C.; Suyu, S.H.; Chen, G.C.-F.; Rusu, C.E.; Millon, M.; Sluse, D.; Bonvin, V.; Fassnacht, C.D.; Taubenberger, S.; Auger, M.W.; et al. H0LiCOW—XIII. A 2.4 percent measurement of H_0 from lensed quasars: 5.3σ tension between early- and late-Universe probes. *Mon. Not. R. Astron. Soc.* **2020**, *498*, 1420–1439. [[CrossRef](#)]
23. Mooley, K.P.; Deller, A.T.; Gottlieb, O.; Nakar, E.; Hallinan, G.; Bourke, S.; Frail, D.A.; Horesh, A.; Corsi, A.; Hotokezaka, K. Superluminal motion of a relativistic jet in the neutron-star merger GW170817. *Nature* **2018**, *561*, 355–359. [[CrossRef](#)]
24. The LIGO Scientific Collaboration and The Virgo Collaboration; The 1M2H Collaboration; The Dark Energy Camera GW-EM Collaboration and the DES Collaboration; The DLT40 Collaboration; The Las Cumbres Observatory Collaboration; The VINROUGE Collaboration; The MASTER Collaboration. A gravitational-wave standard siren measurement of the Hubble constant. *Nature* **2017**, *551*, 85–88. [[CrossRef](#)] [[PubMed](#)]
25. Hotokezaka, K.; Nakar, E.; Gottlieb, O.; Nissanke, S.; Masuda, K.; Hallinan, G.; Mooley, K. P.; Deller, A. T. A Hubble constant measurement from the superluminal motion of the jet in GW170817. *Nat. Astron.* **2019**, *3*, 940–944. [[CrossRef](#)]
26. Wu, Q.; Zhang, G.-Q.; Wang, F.-Y. An 8 percent determination of the Hubble constant from localized fast radio bursts. *Mon. Not. R. Astron. Soc.: Lett.* **2022**, *515*, L1–L5. [[CrossRef](#)]

27. James, C.W.; Ghosh, E.M.; Prochaska, J.X.; Bannister, K.W.; Bhandari, S.; Day, C.K.; Deller, A.T.; Glowacki, M.; Gordon, A.C.; Heintz, K.E.; et al. A measurement of Hubble's Constant using Fast Radio Bursts. *Mon. Not. R. Astron. Soc.* **2022**, *516*, 4862–4881. [[CrossRef](#)]
28. Pesce, D.W.; Braatz, J.A.; Reid, M.J.; Riess, A.G.; Scolnic, D.; Condon, J.J.; Gao, F.; Henkel, C.; Impellizzeri, C.M.V.; Kuo, C.Y.; Lo K.Y. The Megamaser Cosmology Project. XIII. Combined Hubble Constant Constraints. *Astrophys. J. Lett.* **2020**, *891*, L1. [[CrossRef](#)]
29. Reid, J.; Pesce, D.W.; Riess, A.G. An Improved Distance to NGC 4258 and Its Implications for the Hubble Constant. *Astrophys. J. Lett.* **2019**, *886*, L27. [[CrossRef](#)]
30. Kuo, C.Y.; Braatz, J.A.; Lo K.Y.; Reid, M.J.; Suyu, S.H.; Pesce, D.W.; Condon, J.J.; Henkel, C.; Impellizzeri, C.M.V. The Megamaser Cosmology Project. VI. Observations of NGC 6323. *Astron. J.* **2015**, *800*, 26. [[CrossRef](#)]
31. Freedman, W.L.; Madore, B.F.; Hatt, D.; Hoyt, T.J.; Jang, I.S.; Beaton, R.L.; Burns, C.R.; Lee, M.G.; Monson, A.J.; Neeley, J.R.; et al. The Carnegie-Chicago Hubble Program. VIII. An Independent Determination of the Hubble Constant Based on the Tip of the Red Giant Branch. *Astron. J.* **2019**, *882*, 34. [[CrossRef](#)]
32. Freedman, W.L.; Madore, B.F.; Hoyt, T.; Jang, I.S.; Beaton, R.; Lee, M.G.; Monson, A.; Neeley, J.; Jeffrey, R. Calibration of the Tip of the Red Giant Branch. *Astron. J.* **2020**, *891*, 57. [[CrossRef](#)]
33. Freedman, W.L. Measurements of the Hubble Constant: Tensions in Perspective. *Astron. J.* **2021**, *919*, 16. [[CrossRef](#)]
34. Addison, G.E.; Watts, D.J.; Bennett, C.L.; Halpern, M.; Hinshaw, G.; Weil, J.L. Elucidating Λ CDM: Impact of Baryon Acoustic Oscillation Measurements on the Hubble Constant Discrepancy. *Astron. J.* **2021**, *853*, 119. [[CrossRef](#)]
35. Moresco, M.; Amati, L.; Amendola, L.; Birrer, S.; Blakeslee, J.P.; Cantiello, M.; Cimatti, A.; Darling, J.; Valle, M.D.; Fishbach, M.; et al. Unveiling the Universe with emerging cosmological probes. *Living Rev. Relativ.* **2022**, *25*, 6. [[CrossRef](#)]
36. Suyu, S.H.; Bonvin, V.; Courbin, F.; Fassnacht, C.D.; Rusu, C.E.; Sluse, D.; Treu, T.; Wong, K.C.; Auger, M.W.; Ding, X.; et al. H0LICOW—I. H0 Lenses in COSMOGRAIL's Wellspring: Program overview. *Mon. Not. R. Astron. Soc.* **2017**, *468*, 2590–2604. [[CrossRef](#)]
37. Zhang, X.; Huang, Q.G. Measuring H_0 from low- z datasets. *Sci. China Phys. Mech. Astron.* **2020**, *63*, 290402. [[CrossRef](#)]
38. Kazantzidis, L.; Perivolaropoulos, L. Evolution of the $f\sigma_8$ tension with the Planck15/ Λ CDM determination and implications for modified gravity theories. *Phys. Rev. D* **2018**, *97*, 103503. [[CrossRef](#)]
39. Linder, E.V. Probing gravitation, dark energy, and acceleration. *Phys. Rev. D* **2004**, *70*, 023511. [[CrossRef](#)]
40. Chevallier, M.; Polarski, D. Accelerating universes with scaling dark matter. *Int. J. Mod. Phys. D* **2001**, *10*, 213–223. [[CrossRef](#)]
41. Linder, E.V. Exploring the Expansion History of the Universe. *Phys. Rev. Lett.* **2003**, *90*, 091301. [[CrossRef](#)] [[PubMed](#)]
42. Ross, A.J.; Samushia, L.; Howlett, C.; Percival, W.J.; Burden, A.; Manera, M. The clustering of the SDSS DR7 main Galaxy sample—I. A 4 per cent distance measure at $z = 0.15$. *Mon. Not. R. Astron. Soc.* **2015**, *449*, 835–847. [[CrossRef](#)]
43. Alam, S.; Ata, M.; Bailey, S.; Beutler, F.; Bizyaev, D.; Blazek, J.A.; Bolton, A.S.; Brownstein, J.R.; Burden, A.; Chuang, C.-H.; et al. The clustering of galaxies in the completed SDSS-III Baryon Oscillation Spectroscopic Survey: Cosmological analysis of the DR12 galaxy sample. *Mon. Not. R. Astron. Soc.* **2017**, *470*, 2617–2652. [[CrossRef](#)]
44. Gil-Marín, H.; Bautista, J.E.; Paviot, R.; Vargas, M.; De la Torre, S.; Fromenteau, S.; Alam, S.; Avila, S.; Burtin, E.; Chuang, C.-H.; et al. The Completed SDSS-IV extended Baryon Oscillation Spectroscopic Survey: Measurement of the BAO and growth rate of structure of the luminous red galaxy sample from the anisotropic power spectrum between redshifts 0.6 and 1.0. *Mon. Not. R. Astron. Soc.* **2020**, *498*, 2492–2531. [[CrossRef](#)]
45. Raichoor, A.; De Mattia, A.; Ross, A.J.; Zhao, C.; Alam, S.; Avila, S.; Bautista, J.; Brinkmann, J.; Brownstein, J.R.; Burtin, E.; et al. The completed SDSS-IV extended Baryon Oscillation Spectroscopic Survey: Large-scale structure catalogues and measurement of the isotropic BAO between redshift 0.6 and 1.1 for the Emission Line Galaxy Sample. *Mon. Not. R. Astron. Soc.* **2021**, *500*, 3254–3274. [[CrossRef](#)]
46. Hou, J.; Sanchez, A.G.; Ross, A.J.; Smith, A.; Neveux, R.; Bautista, J.; Burtin, E.; Zhao, C.; Scoccamarro, R.; Dawson, K.S.; et al. The completed SDSS-IV extended Baryon Oscillation Spectroscopic Survey: BAO and RSD measurements from anisotropic clustering analysis of the quasar sample in configuration space between redshift 0.8 and 2.2. *Mon. Not. R. Astron. Soc.* **2021**, *500*, 1201–1221. [[CrossRef](#)]
47. du Mas des Bourboux, H.; Rich, J.; Font-Ribera, A.; de Sainte Agathe, V.; Farr, J.; Etourneau, T.; Le Goff, J.-M.; Cuceu, A.; Balland, C.; Bautista, J. E.; et al. The Completed SDSS-IV Extended Baryon Oscillation Spectroscopic Survey: Baryon Acoustic Oscillations with Ly α Forests. *Astron. J.* **2020**, *901*, 153. [[CrossRef](#)]
48. DES Collaboration. Dark Energy Survey Year 3 results: A 2.7 percent measurement of baryon acoustic oscillation distance scale at redshift 0.835. *Phys. Rev. D* **2022**, *105*, 043512. [[CrossRef](#)]
49. Sridhar, S.; Song, Y.-S.; Ross, A. J.; Zhou, R.; Newman, J. A.; Chuang, C.-H.; Blum, R.; Gaztanaga, E.; Landriau, M.; Prada, F. Clustering of LRGs in the DECaLS DR8 Footprint: Distance Constraints from Baryon Acoustic Oscillations Using Photometric Redshifts. *Astron. J.* **2020**, *904*, 69. [[CrossRef](#)]
50. Beutler, F.; Blake, C.; Colless, M.; Jones, D. H.; Staveley-Smith, L.; Campbell, L.; Parker, Q.; Saunders, W.; Watson, F. The 6dF Galaxy Survey: Baryon acoustic oscillations and the local Hubble constant. *Mon. Not. R. Astron. Soc.* **2011**, *416*, 3017–3032. [[CrossRef](#)]
51. Handley, W.J.; Hobson, M.P.; Lasenby, A.N. POLYCHORD: Nested sampling for cosmology. *Mon. Not. R. Astron. Soc. Lett.* **2015**, *450*, L61–L65. [[CrossRef](#)]

52. Riess, A.G.; Anand, G.S.; Yuan, W.; Casertano, S.; Dolphin, A.; Macri, L.M.; Breuval, L.; Scolnic, D.; Perrin, M.; Anderson, R.I. Crowded No More: The Accuracy of the Hubble Constant Tested with High-resolution Observations of Cepheids by JWST. *Astrophys. J. Lett.* **2023**, *956*, L18. [[CrossRef](#)]
53. Alam, S.; Aubert, M.; Avila, S.; Ball, C.; Bautista, J.E.; Bershad, M.A.; Bizyaev, D.; Blanton, M.R.; Bolton, A.S.; Bovy, J.; et al. Completed SDSS-IV extended Baryon Oscillation Spectroscopic Survey: Cosmological implications from two decades of spectroscopic surveys at the Apache Point Observatory. *Phys. Rev. D* **2021**, *103*, 083533. [[CrossRef](#)]
54. Wang, Y.; Zhao, G.; Chuang, C.; Ross, A. J.; Percival, W. J.; Gil-Marín, H.; Cuesta, A. J. The clustering of galaxies in the completed SDSS-III Baryon Oscillation Spectroscopic Survey: Tomographic BAO analysis of DR12 combined sample in configuration space. *Mon. Not. R. Astron. Soc.* **2017**, *469*, 3762–3774. [[CrossRef](#)]
55. Zhao, G.-B.; Wang, Y.; Taruya, A.; Zhang, W.; Gil-Marín, H.; de Mattia, A.; Ross, A. J.; Raichoor, A.; Zhao, C.; Percival, W. J.; et al. The completed SDSS-IV extended Baryon Oscillation Spectroscopic Survey: A multitracer analysis in Fourier space for measuring the cosmic structure growth and expansion rate. *Mon. Not. R. Astron. Soc.* **2021**, *504*, 33–52. [[CrossRef](#)]
56. Scolnic, D.M.; Jones, D.O.; Rest, A.; Pan, Y.C.; Chornock, R.; Foley, R.J.; Huber, M.E.; Kessler, R.; Narayan, G.; Riess, A.G.; et al. The Complete Light-curve Sample of Spectroscopically Confirmed SNe Ia from Pan-STARRS1 and Cosmological Constraints from the Combined Pantheon Sample. *Astron. J.* **2018**, *859*, 101. [[CrossRef](#)]
57. Zhang, C.; Zhang, H.; Yuan, S.; Liu, S.; Zhang, T.-J.; Sun, Y.-C. Four new observational H(z) data from luminous red galaxies in the Sloan Digital Sky Survey data release seven. *Res. Astron. Astrophys.* **2014**, *14*, 1221 [[CrossRef](#)]
58. Simon, J.; Verde, L.; Jimenez, R. Constraints on the redshift dependence of the dark energy potential. *Phys. Rev. D* **2005**, *71*, 123001. [[CrossRef](#)]
59. Moresco, M.; Cimatti, A.; Jimenez, R.; Pozzetti, L.; Zamorani, G.; Bolzonella, M.; Dunlop, J.; Lamareille, F.; Mignoli, M.; Pearce, H.; et al. Improved constraints on the expansion rate of the Universe up to $z \approx 1.1$ from the spectroscopic evolution of cosmic chronometers. *J. Cosmol. Astropart. Phys.* **2012**, *8*, 6. [[CrossRef](#)]
60. Moresco, M.; Pozzetti, L.; Cimatti, A.; Jimenez, R.; Maraston, C.; Verde, L.; Thomas, D.; Citro, A.; Tojeiro, R.; Wilkinson, D. A 6 percent measurement of the Hubble parameter at $z \approx 0.45$: Direct evidence of the epoch of cosmic re-acceleration. *J. Cosmol. Astropart. Phys.* **2016**, *5*, 14. [[CrossRef](#)]
61. Ratsimbazafy, A.L.; Loubser, S.I.; Crawford, S.M.; Cress, C.M.; Bassett, B.A.; Nichol, R.C.; Väisänen, P. Age-dating luminous red galaxies observed with the Southern African Large Telescope. *Mon. Not. R. Astron. Soc.* **2017**, *467*, 3239–3254. [[CrossRef](#)]
62. Stern, D.; Jimenez, R.; Verde, L.; Kamionkowski, M.; Stanford, S.A. Cosmic chronometers: Constraining the equation of state of dark energy. I: H(z) measurements. *J. Cosmol. Astropart. Phys.* **2010**, *2*, 8. [[CrossRef](#)]
63. Borghi, N.; Moresco, M.; Cimatti, A. Toward a Better Understanding of Cosmic Chronometers: A New Measurement of H(z) at $z \approx 0.7$. *Astrophys. J. Lett.* **2022**, *928*, L4. [[CrossRef](#)]
64. Jiao, K.; Borghi, N.; Moresco, M.; Zhang, T.-J. New Observational H(z) Data from Full-spectrum Fitting of Cosmic Chronometers in the LEGA-C Survey. *Astrophys. J. Suppl. Ser.* **2023**, *265*, 48. [[CrossRef](#)]
65. Moresco, M. Raising the bar: New constraints on the Hubble parameter with cosmic chronometers at $z \approx 2$. *Mon. Not. R. Astron. Soc.: Lett.* **2015**, *450*, L16–L20. [[CrossRef](#)]
66. Nunes, R.C.; Yadav, S.K.; Jesus, J.F.; Bernui, A. Cosmological parameter analyses using transversal BAO data. *Mon. Not. R. Astron. Soc.* **2020**, *497*, 2133–2141. [[CrossRef](#)]
67. Nunes, R.C.; Bernui, A. BAO signatures in the 2-point angular correlations and the Hubble tension. *Eur. Phys. J. C.* **2020**, *80*, 1025. [[CrossRef](#)]
68. Verde, L.; Bernal, J.L.; Heavens, A.F.; Jimenez, R. The length of the low-redshift standard ruler. *Mon. Not. R. Astron. Soc.* **2017**, *467*, 731–736. [[CrossRef](#)]
69. Lemos, T.; Ruchika; Carvalho, J.C.; Alcaniz, J. Low-redshift estimates of the absolute scale of baryon acoustic oscillations. *Eur. Phys. J. C* **2023**, *83*, 495. [[CrossRef](#)]
70. Pogosian, L.; Zhao, G.-B.; Jedamzik, K. Recombination-independent Determination of the Sound Horizon and the Hubble Constant from BAO. *Astrophys. J. Lett.* **2020**, *904*, L7. [[CrossRef](#)]
71. Akaike, H. A new look at the statistical model identification. *IEEE Trans. Autom. Control.* **1974**, *19*, 716–723. [[CrossRef](#)]
72. Schwarz, G. Estimating the Dimension of a Model. *Ann. Statist.* **1978**, *6*, 461–464. [[CrossRef](#)]

Disclaimer/Publisher’s Note: The statements, opinions and data contained in all publications are solely those of the individual author(s) and contributor(s) and not of MDPI and/or the editor(s). MDPI and/or the editor(s) disclaim responsibility for any injury to people or property resulting from any ideas, methods, instructions or products referred to in the content.